

# ISO-LWS observations of Herbig Ae/Be stars<sup>\*</sup>

## II. Molecular lines

T. Giannini<sup>1,2,3</sup>, D. Lorenzetti<sup>2</sup>, E. Tommasi<sup>4</sup>, B. Nisini<sup>3</sup>, M. Benedettini<sup>3</sup>, S. Pezzuto<sup>3</sup>, F. Strafella<sup>5</sup>, M. Barlow<sup>6</sup>, P.E. Clegg<sup>7</sup>, M. Cohen<sup>8</sup>, A.M. Di Giorgio<sup>3</sup>, R. Liseau<sup>9</sup>, S. Molinari<sup>10</sup>, F. Palla<sup>11</sup>, P. Saraceno<sup>3</sup>, H.A. Smith<sup>12</sup>, L. Spinoglio<sup>3</sup>, and G.J. White<sup>7</sup>

<sup>1</sup> Istituto Astronomico, Università La Sapienza, via Lancisi 29, I-00161 Roma, Italy

<sup>2</sup> Osservatorio Astronomico di Roma, via Frascati 33, I-00040 Monte Porzio, Italy

<sup>3</sup> Istituto di Fisica Spazio Interplanetario – CNR Area Ricerca Tor Vergata, via Fosso del Cavaliere, I-00133 Roma, Italy

<sup>4</sup> Agenzia Spaziale Italiana, via di Villa Patrizi 13, I-00161 Roma, Italy

<sup>5</sup> Dipartimento di Fisica, Università di Lecce, I-73100 Lecce, Italy

<sup>6</sup> Department of Physics and Astronomy, University College London, Gower Street, London WC1E 6BT, UK

<sup>7</sup> Queen Mary and Westfield College, University of London, Mile End Road, London E1 4NS, UK

<sup>8</sup> Radio Astronomy Laboratory, 601 Campbell Hall, University of California, Berkeley, CA 94720, USA

<sup>9</sup> Stockholm Observatory, S-133 36 Saltsjöbaden, Sweden

<sup>10</sup> IPAC/Caltech, MS 100-22, Pasadena, CA, USA

<sup>11</sup> Osservatorio Astrofisico di Arcetri, Largo E.Fermi 5, I-50125 Firenze, Italy

<sup>12</sup> Harvard-Smithsonian Centre for Astrophysics, 60 Garden Street, Cambridge, MA 02138, USA

Received 25 November 1998 / Accepted 11 March 1999

**Abstract.** We present the first ISO-LWS observations of the molecular FIR lines in 3 out of a sample of 11 Herbig Ae/Be stars (HAEBE), namely IRAS12496-7650, RCrA and LkH $\alpha$ 234. High-J rotational CO lines (from  $J_{\text{up}} = 14$  to  $J_{\text{up}} = 19$ ) have been observed in all the spectra, while two (at 79  $\mu\text{m}$  and 84  $\mu\text{m}$ ) and three OH lines (at 71  $\mu\text{m}$ , 79  $\mu\text{m}$  and 84  $\mu\text{m}$ ) were detected in LkH $\alpha$ 234 and RCrA respectively.

For all sources the molecular emission has been consistently fitted with a Large Velocity Gradient (LVG) model and it results originated in a warm ( $T \gtrsim 200$  K) and dense ( $n_{\text{H}_2} \gtrsim 10^5 \text{ cm}^{-3}$ ) gas located in very compact regions having diameters of few hundreds of AU.

These three sources are those with the highest density among the stars of the sample; this suggests that the molecular emission arises in regions showing density peaks.

By comparing the observed cooling ratios with model predictions, we find that the FUV radiation from the central source (or from a more embedded companion) is the most likely responsible for the line excitation. At least for the sources where OH has been observed, the contribution of shocks to the line emission can be reasonably ruled out because of the absence in the spectra of any water vapour lines, in contrast with the predictions for molecular emission coming from warm shocked environments.

**Key words:** stars: circumstellar matter – stars: pre-main sequence – infrared: ISM: lines and bands – infrared: stars

### 1. Introduction

Considerable efforts have been made in recent years to both observe and model the inter-relationships between Herbig Ae/Be stars (HAEBE) and their surrounding environment. These pre-main-sequence stars, which are the higher mass counterparts of T Tauri stars, represent an intermediate luminosity sample for studying the interactions with the parent cloud material, which is still present in this evolutionary phase. Molecular line observations are the most suitable probe to investigate both the cooling and kinematics of low temperature, high density gas. Because of the limitations imposed by ground-based facilities, most molecular line observations have been devoted to searching for (i) (bipolar) molecular outflows by means of  $^{12}\text{CO}$  and  $^{13}\text{CO}$  J=1-0 mapping (Cantó et al. 1984; Levreault 1988), and (ii) highly collimated jets through the quadrupole  $\text{H}_2$  roto-vibrational transition  $v=1-0$  S(1) (Mundt & Ray 1994).

Other molecular transitions of CS, SO, HCN,  $\text{H}_2\text{CO}$ ,  $\text{HCO}^+$  have been occasionally observed towards a few HAEBE and in two cases (V645 Cyg and LkH $\alpha$ 234)  $\text{H}_2\text{O}$  maser emission was detected (Lada et al. 1981; Rodriguez et al. 1980). A systematic survey of 8 HAEBE in the J=1-0 transition of  $\text{HCO}^+$ , HCN and their isotopomers, was conducted by Scappini et al. (1994). Fuente et al. (1990, 1992) studied in  $^{12}\text{CO}$ ,  $^{13}\text{CO}$  and  $\text{NH}_3$  the clouds associated with HAEBE to examine the effects of the young stars on the surrounding gas. More recently Fuente et

Send offprint requests to: T. Giannini (teresa@coma.mporzio.astro.it)

<sup>\*</sup> Based on observations with ISO, an ESA project with instruments funded by ESA Member States and with the participation of ISAS and NASA

al. (1998) mapped at high spatial resolution an extended region around 14 HAEBE in the  $^{13}\text{CO}$  1-0 and CS 3-2 molecular lines, pointing out a progressive dispersal of the dense gas during the evolution of the stars towards the main sequence. This gas, situated in the circumstellar (CS) neighbourhood, is exposed to the far-UV radiation from both the central exciting star and the interstellar field; moreover in many cases an additional interaction with the stellar wind results in gas heating by means of C/J-shocks. According to model predictions (e.g. Kaufman & Neufeld 1996, Hollenbach & McKee 1989), molecular gas cooling is dominated by emission in the high-J CO,  $\text{H}_2\text{O}$ , OH rotational transitions. These lines lie in a spectral range (50–200  $\mu\text{m}$ ) where only airplane observations had been performed in the past years. Now the spectroscopic capabilities offered by ISO (Infrared Space Observatory), and in particular by the Long Wavelength Spectrometer (LWS), have allowed us to perform the first unbiased spectral survey in the FIR (45–197  $\mu\text{m}$ ) of a significant sample of HAEBE, providing the opportunity to investigate from a statistical point of view the mechanisms at the origin of the molecular gas excitation.

Thus, the main aims of the present work are threefold:

- to search for molecular lines in the LWS wavelength range and to understand how their presence (or absence) is related to the properties of both the central HAEBE and the circumstellar environment;
- to derive from line intensities and intensity ratios the physical properties (density and temperature) of the emitting gas;
- to compare the results with current model predictions in order to recognise the dominant mechanism(s) of the excitation.

## 2. Observations and data reduction

We have investigated a sample of 11 HAEBE stars as part of the guaranteed time programme observations carried out with the Long Wavelength Spectrometer (LWS: Clegg et al. 1996) on board the Infrared Space Observatory (ISO: Kessler et al. 1996). The definition of the sample, the pointing procedures and the Journal of observations are given in Lorenzetti et al. 1999 (hereinafter Paper I). The spectra were obtained with the LWS AOT01 full grating scan mode (i.e. 43–197  $\mu\text{m}$  wavelength range, resolution  $R \sim 200$ , instrumental beam size of  $\sim 80$  arcsec), using the “fast scanning” option and a sampling of 1/4 of the spectral resolution element. The flux calibration was derived on the basis of Uranus observations (accuracy of about 30%, Swinyard et al. 1996), while the uncertainty in wavelength calibration is about 25% of the resolution element (i.e. 0.07  $\mu\text{m}$  and 0.15  $\mu\text{m}$  for the short (43–90  $\mu\text{m}$ ) and the long (90–197  $\mu\text{m}$ ) wavelength ranges respectively). The spectra are composed by ten sub-spectra corresponding to the ten detectors. The preliminary analysis was made using the version 7 of the off line pipeline (OLP-V7); the raw data were then processed with an internal pipeline for de-glitching spurious signals introduced by the impact of cosmic rays and for correcting the data from low-frequency fringes, which are a consequence of interference by off axis signals (Swinyard et al. 1996). The final spectra were

obtained by averaging the different spectral scans and re-scaling the ten sub-spectra using the average of overlapping regions.

## 3. Results

Out of the 11 observed HAEBE we found molecular emission (according to the detection criteria reported in Paper I) in three objects, namely IRAS12496-7650, RCrA and LkH $\alpha$ 234. In each of these sources at least five transitions of the CO pure rotational lines (with  $J_{\text{up}}$  between 14 and 19) were observed; in addition, we also detected in RCrA the OH  $^2\Pi_{\Omega=1/2, J=7/2} \rightarrow ^2\Pi_{\Omega=1/2, J=5/2}$ ,  $^2\Pi_{\Omega=1/2, J=1/2} \rightarrow ^2\Pi_{\Omega=3/2, J=3/2}$ ,  $^2\Pi_{\Omega=3/2, J=7/2} \rightarrow ^2\Pi_{\Omega=3/2, J=5/2}$  lines at 71  $\mu\text{m}$ , 79  $\mu\text{m}$  and 84  $\mu\text{m}$  respectively, while in LkH $\alpha$ 234 only the 79  $\mu\text{m}$  and 84  $\mu\text{m}$  lines were detected. The line fluxes were measured from the defringed single detector spectra by gaussian fitting the spectral profiles. For all the lines, the FWHM were comparable with the instrumental resolution element width (i.e. 0.29  $\mu\text{m}$  and 0.6  $\mu\text{m}$  for the SW and LW detectors respectively) except the OH 79  $\mu\text{m}$  and 84  $\mu\text{m}$  lines, whose FWHM’s were broader because of the unresolved contribution of the fine structure lines due to the  $\Lambda$  doubling splitting of the levels. Fig. 1 shows the continuum subtracted (by means of first or second order polynomial fitting) parts of the spectra where the molecular emission has been revealed. In Table 1 we report, for each source (Column 1), the identified molecular lines (Column 2), along with the observed and rest vacuum central line wavelengths (Columns 3 and 4) and the integrated fluxes with the relative  $1\sigma$  statistical uncertainties estimated from the rms in the adjacent baseline (Column 5). Some of the molecular line fluxes of the three HAEBE are also reported in Paper I, in which they have been computed using raw spectra obtained from the OLP-V6; moreover, a preliminary analysis of the IRAS12496-7650 line fluxes has been already published in Nisini et al. (1996) (OLP-V4). The comparison between the measured fluxes obtained from the V6 and V7 pipelines spectra shows agreement within the errors, although the improved data analysis performed in version 7 revealed further molecular lines which were previously undetected. On the contrary, the three CO line fluxes and the line intensities ratios of IRAS12496-7650 (from  $J_{\text{up}}=15$  to  $J_{\text{up}}=17$ ) published in Nisini et al. (1996), are not compatible with the new ones (being different by  $\sim 50\%$ ), probably because of the preliminary flux calibration performed in the OLP-V4. Nonetheless, the indication that these three CO lines trace the peak of the flux density distribution remains valid.

## 4. Line emission fitting

In order to understand the processes involved in the excitation of the molecular material, we have estimated the physical parameters of the emitting gas. We solved the equations of statistical equilibrium for the level populations by adopting the standard approximation of a Large Velocity Gradient (LVG) regime in a plane-parallel geometry. For the CO model we consider the level populations of the first 60 rotational levels, disregarding the vibrational transitions because they quite marginally contribute to

**Table 1.** Molecular line fluxes – V7 Off Line Pipeline

Source	Line Identification	$\lambda_{vac}$ ( $\mu\text{m}$ )	$\lambda_{obs}$ ( $\mu\text{m}$ )	$F \pm \Delta F$ ( $10^{-19} \text{ W cm}^{-2}$ )
<b>IRAS12496-7650</b>	CO 19→18	137.20	137.03	0.30±0.07
	CO 18→17	144.76	144.71	0.37±0.08
	CO 17→16	153.27	153.29	0.56±0.05
	CO 16→15	162.81	162.71	0.49±0.06
	CO 15→14	173.63	173.64	0.54±0.06
	CO 14→13	186.00	186.01	0.6 ± 0.2
<b>RCrA</b>	OH ${}^2\Pi_{\Omega=1/2, J=7/2} \rightarrow {}^2\Pi_{\Omega=1/2, J=5/2}$	71.17	71.20	3 ± 1
	OH ${}^2\Pi_{\Omega=1/2, J=1/2} \rightarrow {}^2\Pi_{\Omega=3/2, J=3/2}$	79.15	79.12	9 ± 1
	OH ${}^2\Pi_{\Omega=3/2, J=7/2} \rightarrow {}^2\Pi_{\Omega=3/2, J=5/2}$	84.51	84.52	9 ± 1
	CO 19→18	137.20	137.03	3.8 ± 0.9
	CO 18→17	144.76	-	< 4.0
	CO 17→16	153.27	153.41	5.4±0.8
	CO 16→15	162.81	162.87	5.9±0.5
	CO 15→14	173.63	173.54	6.0±0.8
	CO 14→13	186.00	185.89	6±1
<b>LkH<math>\alpha</math>234</b>	OH ${}^2\Pi_{\Omega=1/2, J=1/2} \rightarrow {}^2\Pi_{\Omega=3/2, J=3/2}$	79.15	79.19	3.0 ± 0.5
	OH ${}^2\Pi_{\Omega=3/2, J=7/2} \rightarrow {}^2\Pi_{\Omega=3/2, J=5/2}$	84.51	84.52	4.0 ± 1.0
	CO 19→18	137.20	137.03	1.4 ± 0.4
	CO 18→17 <sup>†</sup>	144.76	144.80	2.0±0.5
	CO 17→16	153.27	153.21	1.9±0.6
	CO 16→15	162.81	162.93	2.2±0.3
	CO 15→14	173.63	173.69	1.6±0.3
	CO 14→13	186.00	185.89	1.5±0.3

<sup>†</sup> Line deblended with the [OI] 145  $\mu\text{m}$  line.

the observed line intensities. The collisional downward rates by impacts of  $\text{H}_2$  molecules for each pair of levels with  $J_{\text{up}} \leq 60$  and  $100 \leq T \leq 2000$  K are computed from the  $\gamma_{J0}$  coefficients, which represent the de-excitation rates from a level  $J$  to the ground level 0, taken from McKee et al. (1982). Upward rates are computed using the principle of detailed balance. Radiative decay rates are taken from Chackerian & Tipping (1983).

For the OH model we consider the first 20 rotational levels, accounting for  $\Lambda$  doubling splitting of the levels, but disregarding further splitting due to the hyperfine structure. The collisional downward rates are taken from Offer & van Dishoeck (1992), while the upward rates are computed with the same method as before. The radiative decays were derived using the HITRAN catalogue (Rothman et al. 1987). At the moment, radiative excitation by dust emission has not been taken into account in our code; however, this contribution is significant only at gas temperatures about a factor of 4 lower than those we estimate from our fits (Melnick et al. 1987).

The model depends on a relatively large number of free parameters: gas kinetic temperature, density, intrinsic linewidth, column density and filling-factor; this circumstance, along with the relatively high uncertainties in the line flux determinations, does not permit a unique definition of the physical conditions of the emitting gas. In principle, because we observe lines produced by two molecular species, we could independently model both the OH and the CO emission; unfortunately, the small num-

ber of OH lines detected prevents a meaningful application of this procedure. Instead, the data were fitted using only the CO line fluxes, then checking for compatibility of the estimated gas temperature and density with the observed OH line fluxes. The adopted procedure was the following: we assumed that the linewidth was equal to the maximum velocity of the extended CO outflows; then the observed CO line flux distribution as a function of  $J_{\text{up}}$  is used to constrain the gas temperature and density and to define the optical thickness of the lines. Since all the CO lines turn out to be optically thin, the results marginally depend on the choice of the velocity width, validating *a posteriori* the assumption on the adopted value. The absolute flux level depends both on the CO column density ( $N_{\text{CO}}$ ) and the beam filling factor, so that in principle any morphology obtained by varying the angular dimension  $\theta$  and the depth  $dl$  of the emitting region could be accepted; nevertheless it is possible to give a rough estimate of the column density and the filling factor by assuming the width comparable to the depth. Thus, both the absolute flux level and the estimated total gas density (equal to  $N_{\text{H}_2}/dl$ ) has been used to independently derive  $N_{\text{CO}}$  and  $\theta$ , with only the CO abundance with respect to  $\text{H}_2$ ,  $X(\text{CO})$ , being assumed. The OH lines, however, have usually large optical depths: in this case the intensity ratio between two lines with substantially different optical depths can be expressed as a function of the column density (Nisini et al. 1999). In particular, this occurs if at least one of the two line intensities is not thermalised

**Table 2.** Physical parameters of the molecular emission

	IRAS 12496-7650	RCrA	LkH $\alpha$ 234
Gas temperature T (K)	200 $\div$ 750	300 $\div$ 1000	200 $\div$ 900
Gas density $n_{\text{H}_2}$ ( $\text{cm}^{-3}$ )	$4 \cdot 10^6 \div 5 \cdot 10^5$	$4 \cdot 10^6 \div 1.2 \cdot 10^5$	$4 \cdot 10^6 \div 5 \cdot 10^5$
Size (arcsec)	2.5	3.4 $\div$ 10	2.5 $\div$ 3.7
Size (pc)	0.002	0.002 $\div$ 0.007	0.012 $\div$ 0.018
CO column density $N_{\text{CO}}$ ( $\text{cm}^{-2}$ )	$2.4 \cdot 10^{18} \div 3 \cdot 10^{17}$	$3 \cdot 10^{18} \div 4 \cdot 10^{17}$	$1 \cdot 10^{18} \div 4 \cdot 10^{17}$
OH column density $N_{\text{OH}}$ ( $\text{cm}^{-2}$ )	–	$4 \cdot 10^{17}$	$1.5 \cdot 10^{17} \div 4 \cdot 10^{17}$
CO cooling $L_{\text{CO}}$ ( $L_{\odot}$ )	0.003 $\div$ 0.006	0.04	0.6 $\div$ 1
OH cooling $L_{\text{OH}}$ ( $L_{\odot}$ )	–	0.08 $\div$ 0.04	1.1 $\div$ 0.75

at the fitted temperature. This condition is verified for both the sources in which the OH lines have been detected, i.e. RCrA and LkH $\alpha$ 234.

Therefore for these two sources we have relaxed the hypothesis of quasi-spherical geometry and independently constrained both the column density and the angular size. This latter results comparable to the one obtained from the CO lines, thus we can reasonably conclude that CO and OH lines arise from the same region.

Fig. 2 shows the CO fits for each source. The two curves superimposed on the measured fluxes correspond to the possible ranges of temperature and density. The derived parameters are listed in Table 2: the two values refer to the low and high temperature cases respectively; if both determinations are very similar, only a single value is given.

In the next sections we include short descriptions of the environments around each source and discuss the obtained results.

#### 4.1. IRAS 12496-7650

This is the only known intermediate mass YSO in ChaII ( $d \sim 250$  pc). It has continued to undergo irregular and significant near-IR flux variability with amplitude excursions decreasing with wavelength. It appears to be a deeply embedded Ae star surrounded by dusty clumps which irregularly obscure the starlight (Hughes et al. 1991). Knee (1992) found a weak bipolar CO flow associated with this object and argued that the strong CO line wings observed near this source are in no way related with those seen around HH 52–54. IRAS 12496-7650 is thus an outflow YSO but is apparently not responsible for known HHs. It has strong flux densities in the IRAS bands and at 1.3 mm. (Henning et al. 1994, Reipurth et al. 1993). At mid-IR wavelengths the source appears compact (Prusti et al. 1994) and recently Henning et al. (1998), used submm continuum maps to infer a core/envelope structure characterised by having gas mass, column and volume densities of  $0.16 M_{\odot}$ ,  $1.0 \cdot 10^{23} \text{ cm}^{-2}$ ,  $2.9 \cdot 10^6 \text{ cm}^{-3}$ .

Only CO emission (all the lines between  $J_{\text{up}}=14$  and  $J_{\text{up}}=19$ ) has been detected from IRAS12496-7650. The line fluxes are about an order of magnitude lower than those of the other sources, probably as a consequence of the lower bolometric luminosity of this source (that is  $50 L_{\odot}$  compared to 132 and  $283 L_{\odot}$  for RCrA and LkH $\alpha$ 234 respectively). The peak

of the line flux distribution seems to have been traced from the observed lines, constraining the temperature and density to the range  $T=200\text{-}750$  K and  $n_{\text{H}_2}=4 \cdot 10^6 - 5 \cdot 10^5 \text{ cm}^{-3}$  respectively. The model shows that all the observed lines are optically thin. For both the low and high temperature case, in the quasi-spherical approximation, the estimated size of the emitting region results quite similar, amounting to few arcsec (which correspond, at the IRAS12496-7650 distance, to a compact region of about 400 AU). The CO column density ranges between  $2.4 \cdot 10^{18} \div 3 \cdot 10^{17} \text{ cm}^{-2}$  in the low and high temperature case respectively. We note that while the fitted densities are consistent with those inferred from the mm continuum, our hydrogen column density is at least smaller by about an order of magnitude (if  $X(\text{CO}) \leq 10^{-4}$ ).

Although the uncertainty in the value of the dust emissivity makes both evaluations just comparable, it is not surprising that we find smaller column densities since we trace only the warm gas component, while the mm observations refer to the total  $N_{\text{H}_2}$ .

#### 4.2. RCrA

This source is located in one of the closest star forming regions ( $d \sim 150$  pc), and is dominated by the centrally condensed core near RCrA itself. Maps of the whole region have been obtained in the far IR continuum (Wilking et al. 1985) and in molecular line emission:  $\text{H}_2\text{CO}$  (Loren et al. 1983),  $^{12}\text{CO}$  (Levreault 1988) and  $\text{C}^{18}\text{O}$  (Harju et al. 1993), revealing a complex structure containing two superimposed bipolar outflows. The high density region has been traced by mm-wave continuum emission and CS (5-4), (7-6) line emission, which is centered on the embedded source IRS7 (Henning et al. 1998), close to RCrA (about  $20''$  to the SE). It was however not detected in the high sensitivity radio survey of HAEBE (Skinner et al. 1993) probably because of the reduced wind ionization at low effective temperatures. Recently Wilking et al. (1997) obtained both broad (J,H,K) and narrow-band ( $\text{H}_2$ , [FeII]) NIR images of the compact group containing about 10 young stellar objects associated with RCrA; in particular narrow-band images trace the shocked regions associated with HH99 and 104 (Graham 1993).

The RCrA spectrum contains five CO lines with  $J_{\text{up}}$  between 14 and 19 as well as three OH lines. The CO  $J=18 \rightarrow 17$  upper limit has been also measured to check its compatibility

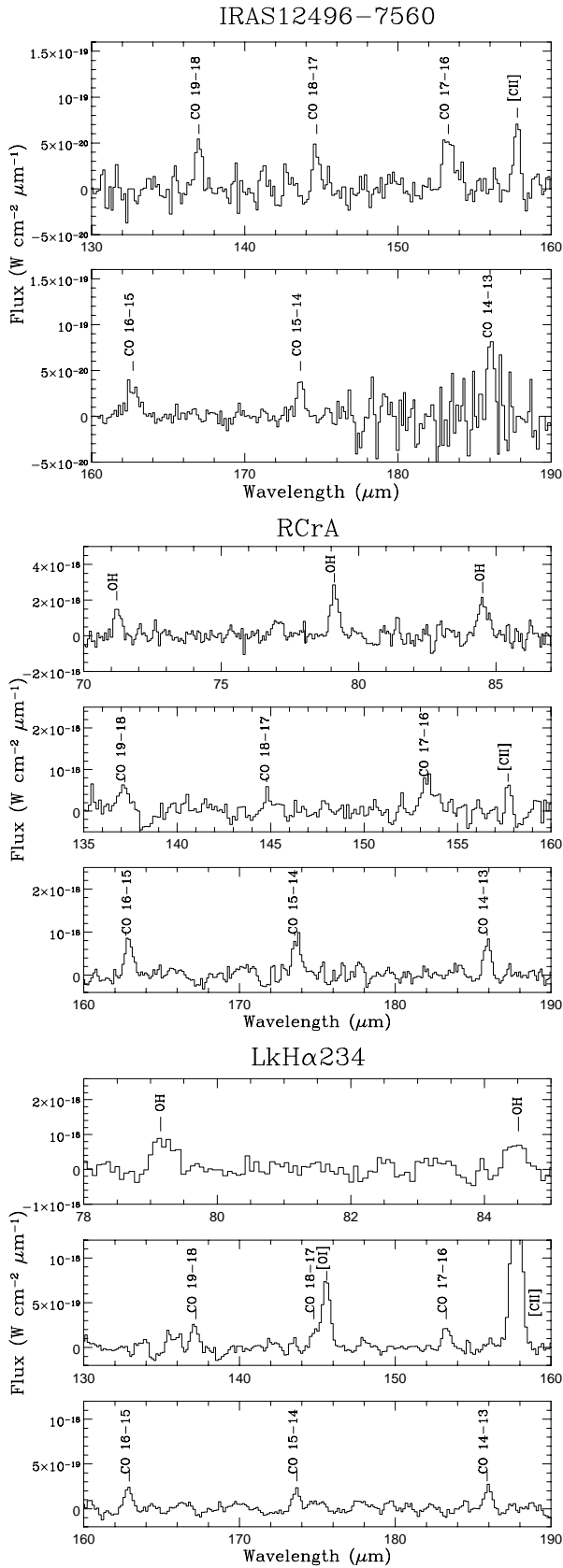


**Fig. 1.** Portions of the LWS continuum subtracted spectra of IRAS 12496-7650 (*top panel*), RCrA (*middle panel*) and LkHa234 (*bottom panel*) where the molecular emission has been detected.

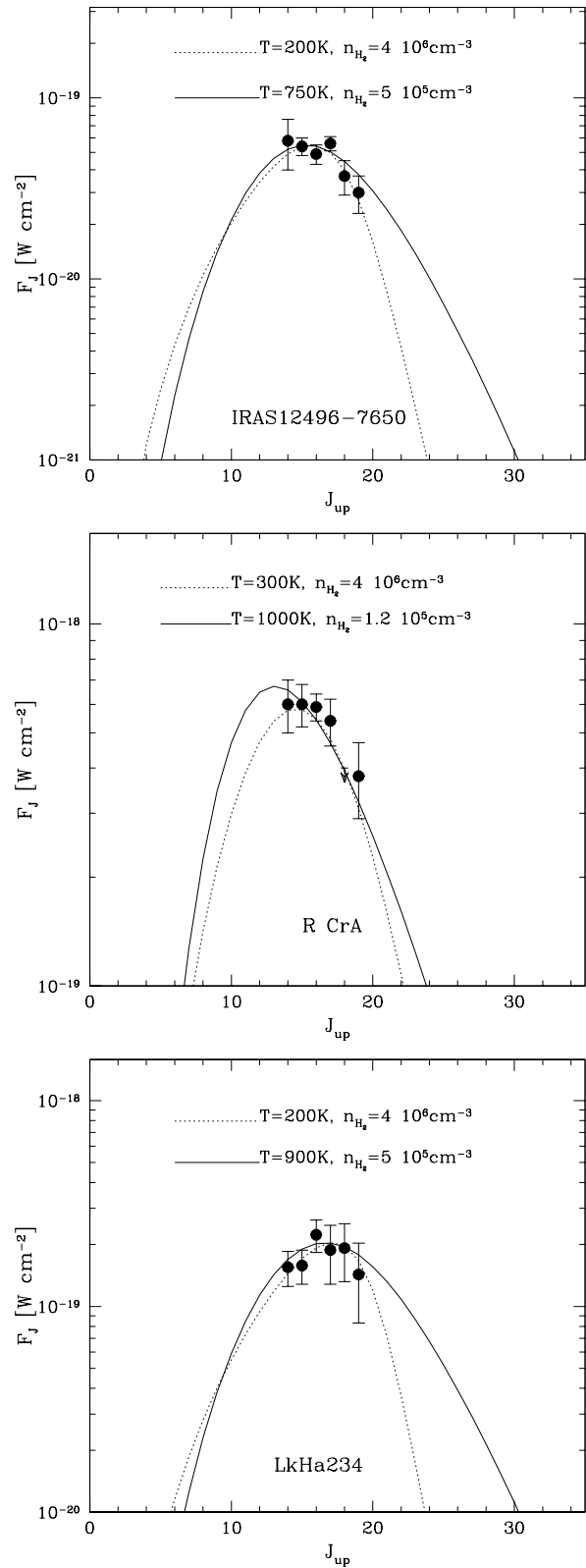


**Fig. 2.** CO line fluxes measured toward IRAS 12496-7650 (*top panel*), RCrA (*middle panel*) and LkHa234 (*bottom panel*) as a function of the rotational quantum number  $J_{\text{up}}$ . The error bars indicate the  $1\sigma$  uncertainties, while the down arrow refers to a  $3\sigma$  upper limit. The dashed and solid lines give the range of possible model fits to the data along with the relative values of temperature and density.

with the shape of the modelled functions. The relatively large uncertainties, especially in the lowest  $J_{\text{up}}$  transitions, allow only gross estimates of the temperature and density, which ranges between  $T=300$  K,  $n_{\text{H}_2} = 4 \cdot 10^6 \text{ cm}^{-3}$  and  $T=1000$  K,  $n_{\text{H}_2} = 1.2 \cdot 10^5 \text{ cm}^{-3}$ . Both these model fits produce optically thin lines. We used this range of physical conditions to fit the three OH lines, and consequently derived the filling factor and the OH and CO column densities. Although both sets of physical conditions are consistent with the observed OH fluxes, the low temperature case seems to better reproduce the data, mainly because it predicts that the undetected OH lines falling in the LWS wavelength range (and in particular the fundamental line at  $119 \mu\text{m}$ ) would have intensities below the  $3\sigma$  noise level. However both models fits predict a similar value for the OH column density ( $\sim 4 \cdot 10^{17} \text{ cm}^{-2}$ ). The size of the emitting region, independently derived from CO and OH lines, ranges between  $3.4 \div 10$  arcsec, corresponding, at the adopted RCrA distance, to a linear dimension of  $4 \cdot 10^2 \div 1.4 \cdot 10^3$  AU. Given this size, a CO column density between  $3 \cdot 10^{18} \text{ cm}^{-2}$  and  $4 \cdot 10^{17} \text{ cm}^{-2}$  is obtained in the low and in the high temperature regime respectively. If  $X(\text{CO})$  is assumed equal to the standard value of  $10^{-4}$ , we derive  $X(\text{OH}) \sim 10^{-5} \div 10^{-4}$ , implying an overabundance of at least two orders of magnitude with respect to the values usually estimated in the local interstellar medium (Irvine et al. 1987). This result will be discussed in Sect. 5.2.

#### 4.3. LkH $\alpha$ 234

Together with the Herbig Be star BD+65 $^\circ$  1637 and a far IR source (Bechis et al. 1978), this source is located in NGC7129 ( $d \sim 1000$  pc), where many phenomena typical of active star formation regions are found: a complex structure of molecular outflows (Edwards & Snell 1983, Mitchell & Matthews 1994), several Herbig-Haro objects and jets (Ray et al. 1990) and water maser emission (Sandell & Olofsson 1981). A deeply embedded companion has been reported by Weintraub et al. (1994) and Cabrit et al. (1997) by means of IR polarisation maps and mid-IR imaging respectively. This companion should be responsible for the CO outflow and the 6 cm radio continuum detected by Skinner et al. (1993). Through  $1100 \mu\text{m}$  mapping, Dent et al. (1989) hypothesised the presence of a dusty ring with a radius of 0.15 pc. LkH $\alpha$ 234 is associated with a large amount of cold dust both in an envelope and a core, whose masses are estimated to be 9.1 and 100  $M_\odot$  respectively, with a total column density  $N_{\text{H}_2} > 6 \cdot 10^{23} \text{ cm}^{-2}$  (Henning et al. 1998). The elongated and curved structure is the edge of a PDR excavated by the nearby ( $\sim 100''$  to the West) BD+65 $^\circ$  1637, as indicated in the  $^{13}\text{CO}$  J=1-0 map of Fuente et al. (1998), who derived a core mass  $\sim 15 M_\odot$ . A quantitative analysis of PDR structure as traced by FIR lines is given in Paper I.

We detected six CO rotational lines in the LkH $\alpha$ 234 spectrum ranging from  $J_{\text{up}}=14$  to  $J_{\text{up}}=19$ , as well as lines of OH at the  $79 \mu\text{m}$  and  $84 \mu\text{m}$ . Despite the large uncertainties of the line fluxes, the CO transitions seem to trace the peak of the flux density distribution versus the  $J_{\text{up}}$  rotational level, providing significant constraints on the emission conditions, which span

from  $T=200$  K and  $n_{\text{H}_2} = 4 \cdot 10^6 \text{ cm}^{-3}$  to  $T=900$  K and  $n_{\text{H}_2} = 5 \cdot 10^5 \text{ cm}^{-3}$ . The OH lines cannot however be so well fitted; nevertheless an estimate of the filling factor and the OH column density could be given, since the two observed lines are expected to be optically thick but have different values of the optical depths.

The derived sizes of CO and OH emitting regions are comparable, ranging approximately from 2.5 to 3.7 arcsec corresponding to a few hundredths of a parsec. If we reasonably assume that these two regions coincide, we find similar values for the CO and OH column densities (for the two temperature regimes,  $1 \cdot 10^{18} \div 4 \cdot 10^{17} \text{ cm}^{-2}$  and  $1.5 \cdot 10^{17} \div 4 \cdot 10^{17} \text{ cm}^{-2}$ , respectively). As for RCrA, this result implies comparable abundances of CO and OH, i.e. OH is overabundant with respect to the interstellar value.

Finally, it is worthwhile to notice that the fitted densities are quite lower than those ( $n_{\text{H}_2} \sim 10^9 \text{ cm}^{-3}$ , Kylafis 1991) expected in the infalling or outflowing gas emitting maser lines. Together with the absence of FIR water lines, this testifies that the region probed by ISO-LWS is by no means related to the H $_2$ O maser discovered nearby LkH $\alpha$ 234.

## 5. Discussion

### 5.1. Occurrence of the molecular emission among Herbig Ae/Be stars

Among the 11 HAEBE stars belonging to our sample, we have clearly detected molecular emission in 3 sources. Marginal detections have also been revealed towards LkH $\alpha$ 198 and in the two out of the four spectra performed along the flow of MWC1080 (Paper I, Tables 3 and 4). From an analysis of the FIR atomic lines, (Paper I, Sect. 5.1 and Fig. 4) the emission from RCrA and IRAS12496-7650 is found located in environments whose densities are greater than all of the other objects of the sample. The estimated values are  $10^5 \div 10^6 \text{ cm}^{-3}$ , while in general for the other sources the densities are  $\sim 10^3 \text{ cm}^{-3}$  or less. LkH $\alpha$ 234 seems to belong to this ‘low density’ group; however our molecular emission analysis does not confirm this result and suggests that the density is of the same order of magnitude as the other two sources.

This coincidence of the molecular emission at the density peaks is also supported by the results given by Fuente et al. (1998). According to them, the HAEBE stars can be classified into three groups, depending on the properties of their circumstellar environments. The first group consists of the stars which are still embedded in the dense core from which they were born and where a great deal of gas column is still present with a relatively high density. From our sample LkH $\alpha$ 234, MWC1080, PV-Cep and LkH $\alpha$ 198 belong to this group; in particular LkH $\alpha$ 234 is the one associated with the dense core having the highest mass. Among these four sources PVCep is the only object for which we did not find any trace of molecular emission. This latter, however, might remain undetectable because of the intrinsic faintness of this source and its very noisy spectrum (see Paper I).

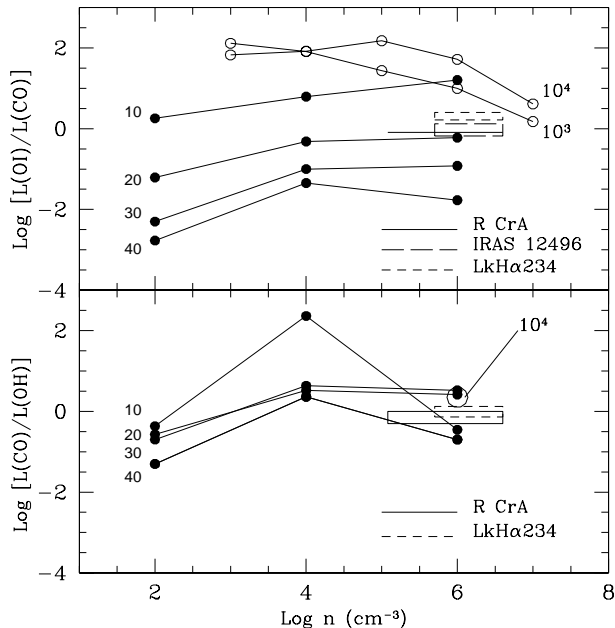


**Fig. 3.** Cooling ratios  $L(\text{OI})/L(\text{CO})$  (top panel) and  $L(\text{CO})/L(\text{OH})$  (bottom panel) vs. density. For the density range inferred from the LVG model (horizontal bars), the fitted cooling ratios (vertical bars) are superimposed onto C-shock (filled circles) and PDR models (open circles). The shock velocities (expressed in  $\text{km s}^{-1}$ ) and the FUV radiation fields (in units of  $G_0$ ) are indicated. The same value for the pre-shock and post-shock density is assumed (see text).

If molecular emission originates close to the density peaks, it could be associated, rather than to the HAEBE itself, to a nearby and more embedded companion, of the kind that has sometimes been discovered in HAEBE neighbourhoods. Indeed Di Francesco et al. (1998), by mapping 50 and 100  $\mu\text{m}$  continuum around HAEBE stars, found that the far-IR emitting dust may not lie immediately around the stars (LkH $\alpha$ 234 is one of the investigated cases); they conclude instead that the FIR emission may originate from dust heated externally or internally by other sources. Because the large ISO-LWS beam does not spatially resolve the mm source IRS7 in the RCrA field (Taylor & Storey 1984) and the embedded companion of LkH $\alpha$ 234 (Weintraub et al. 1994), it would be worthwhile to check whether or not these two less evolved objects could be associated to the molecular emission. Through the relationship  $N_{\text{H}_2} = 1.9 \cdot 10^{21} A_v$  (Bohlin et al. 1978) and by using the column densities we have derived from the fits,  $A_v$  values of about 10 magnitudes can be deduced: these are more typical of embedded objects rather than the few magnitudes of visual extinction usually associated with HAEBE.

### 5.2. Excitation mechanisms for the molecular emission

In all the three sources both shock and quiescent excitation mechanisms have in principle to be taken into account as possibly causing the observed molecular emission. Indeed all these sources have been recognised as drivers of CO molecular outflows and in some cases (RCrA and LkH $\alpha$ 234) associated

Herbig-Haro objects have also been discovered, thus revealing the presence of shock activity. However, contributions to the emission by the photodissociation mechanism cannot be excluded, because of the presence of an enhanced UV field, as confirmed in Paper I by intercomparison of the FIR atomic lines with models of PDRs.

In particular, FIR molecular rotational transitions are expected to be the main gas coolants in non-dissociative C-type shocks (e.g. Draine et al. 1983, Kaufman & Neufeld 1996). These processes are characterised as having velocities  $\lesssim 40 \text{ km s}^{-1}$  and temperatures insufficiently high to dissociate the most abundant molecules, such as  $\text{H}_2$ , CO, OH and  $\text{H}_2\text{O}$ .

Photodissociation regions occur where far-ultraviolet (FUV) radiation dominates the heating, so determining the chemical composition of the gas and its distribution with distance from the central source. If however the gas density is sufficiently high relative to the FUV flux (i.e.  $n/G_0 > 10^2 \text{ cm}^{-3}$ , where  $G_0$  is measured in units of  $1.6 \cdot 10^{-3} \text{ ergs cm}^{-2} \text{ s}^{-1}$ , Habing 1968), the molecular self-shielding will prevent dissociation up to the surface of the molecular cloud (Burton et al. 1990). In these “clumpy” PDRs the contribution to the total gas cooling of the molecular lines becomes comparable or even greater than the atomic fine structure components.

Molecular emission can also occur in dissociative and high temperature J-type shocks with a relative cooling ratio with the ionic/atomic fine structure lines that depends on the pre-shock density conditions (e.g. Hollenbach & McKee 1989). In particular the FIR cooling is largely dominated by the [OI] 63  $\mu\text{m}$  line if  $n_{\text{pre-shock}} \sim 10^4 \text{ cm}^{-3}$  and by the  $\text{H}_2\text{O}$  rotational lines if  $n_{\text{pre-shock}} \gtrsim 10^5 \text{ cm}^{-3}$ . Both these alternatives are not compatible with the observations; we exclude the former because the total luminosity of the CO lines results always greater or at least comparable with the one of [OI] 63  $\mu\text{m}$  line (Paper I, Table 3) and the latter because the predicted cooling ratio  $L(\text{H}_2\text{O})/L(\text{CO})$  is  $\sim 10$ , clearly in contrast with the absence of water lines. Therefore we can reasonably rule out J-type shocks as the origin of the molecular line emission.

To test the remaining alternatives, we compared our observations with C-shocks and dense PDRs model predictions. We show in Fig. 3 the cooling ratios of  $L([\text{OI}]) 63 \mu\text{m}/L(\text{CO})$  (top panel) and  $L(\text{CO})/L(\text{OH})$  (bottom panel) derived from the LVG model as function of the number density. These values are superimposed on C-shock predictions for the different shock velocities of Draine et al. (1983) (filled circles) and on the clumpy PDR models of Burton et al. (1990) for different FUV radiation field (open circles). Although a more recent C-shock model is available in literature (Kaufman & Neufeld 1996), we use the model of Draine et al. because it uniquely provides, at the same time, the molecular and the atomic oxygen cooling rates, thus allowing a more coherent diagnostic with the detected FIR lines. Whereas PDR models and the data are given as a function of the actual density, the C-shock models refer to *pre-shock* density. In this sense, the plot shown in Fig. 3 is fully consistent only if the pre-shock equals the post-shock density value. A more realistic case might be obtained by assuming a compression factor  $n_{\text{post-shock}}/n_{\text{pre-shock}}$  between 10 and 100: accordingly the

C-shock models would shift towards densities increased by the same factor, reinforcing the agreement with the observed data and suggesting that the C-shock mechanism is a possible source of the gas excitation. Whatever is the density compression factor, the estimated velocities result  $\sim 15\text{--}20\text{ km s}^{-1}$ , implying neutral temperatures  $\geq 500\text{ K}$  (Draine et al. 1983).

Nevertheless, in this picture some significant questions remain unresolved. Most importantly, C-type shock models predict that a significant fraction of the gas cooling should be due to emission by water lines as soon as the temperature reaches the threshold value of about  $400\text{ K}$ , as would occur in all sources. At these temperatures, all of the oxygen not fully locked into grains is converted through two subsequent endothermic chemical reactions, firstly into OH, and then, quite quickly, into water (Elitzur & de Jong 1973, Elitzur & Watson 1978). As a consequence of these processes the  $\text{H}_2\text{O}$  abundance increases rapidly, while that of OH is decreased. In particular, for the derived ranges of densities and shock velocities, the smallest expected values of the ratios  $L(\text{H}_2\text{O})/L(\text{OH})$  and  $L(\text{H}_2\text{O})/L(\text{CO})$  are of the order of  $10^2$  and of 10 respectively. These circumstances contrast strongly with our observational findings. A C-shock interpretation would be still reconcilable with the data only in the quite unlikely scenario where the three sources are all being observed during the same very short time phase (about  $100\text{ yr}$  long) during which the OH molecule has not yet been converted into water (Bergin et al. 1997).

On the contrary, the clumpy PDR model seems to provide the only explanation for the observed data.

First of all, the model prescriptions about the ratios  $n/G_0$  are verified in all the objects, as shown by the comparison between our derived densities and the results reported in Paper I about the respective radiation fields.

Secondly, the absence of water lines is fully explained: despite allowing for self-shielding, the dissociation of the  $\text{H}_2\text{O}$  molecule into  $\text{OH} + \text{H}$  cannot be prevented except deep inside the cloud. OH however can more easily survive, since its photodissociation cross section at the  $\text{Ly}\alpha$  wavelength is one order of magnitude less than that of  $\text{H}_2\text{O}$  (van Dishoeck & Dalgarno 1984).

Finally, for the estimated temperatures and densities the clumpy PDR model predicts roughly the following abundance ratios:  $X(\text{CO})/X(\text{H}_2\text{O}) \sim 50$ ,  $X(\text{OH})/X(\text{H}_2\text{O}) \sim 15$ ,  $X(\text{CO})/X(\text{OH}) \sim 3$ . The first two ratios cannot be quantitatively checked with the data because they are below the ISO-LWS detection limits, although well compatible with the upper limits. The third ratio, that relates species directly observed, can be inferred from observations, and our derived value is  $\sim 4$  for both RCrA and LkH $\alpha$ 234.

The remaining question for producing a consistent view of PDR emission deals with the [OI]  $63\ \mu\text{m}$  emission. As already indicated (Fig. 3, top panel) PDR clumpy models can only marginally account for the observed data; in particular they predict more OI luminosity than is observed. This latter is dominated by the  $63\ \mu\text{m}$  transition; this could however be self-absorbed from cold oxygen along the line of sight (Saraceno et al. 1998). Thus, to reconcile the observed data and the model pre-

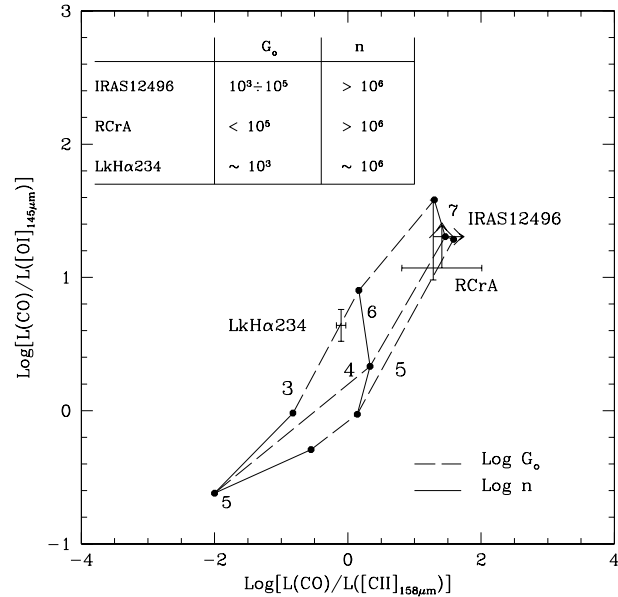


**Fig. 4.** Observed line ratios between molecular CO lines and fine structure [OI]  $145\ \mu\text{m}$  and [CII]  $158\ \mu\text{m}$  superimposed on clumpy PDR models. On the upper left corner the derived values for  $G_0$  and density are given.

dictions, an *ad hoc* assumption on the magnitude of any absorption is needed. This difficulty can be circumvented by exploiting FIR lines other than [OI]  $63\ \mu\text{m}$ . In Fig. 4 we have plotted the ratios  $L(\text{CO})/L([\text{OI}]\ 145\ \mu\text{m})$  vs.  $L(\text{CO})/L([\text{CII}]\ 158\ \mu\text{m})$  superimposed on the Burton et al. models. This plot offers the further advantage of providing a diagnostic of the physical conditions by means of both atomic and molecular line emission. The derived densities and FUV radiation fields are reported in the upper left corner of the same figure. In particular, the derived densities are compatible with those of Table 2.

Summarising, we conclude that strong indications supporting a PDR dominating mechanism are deduced from the observations, although contributions to the emission from C-shocks cannot be definitively excluded, at least for the IRAS12496-7650 source, in which only the CO emission is detected and then no molecular cooling ratio can be derived.

## 6. Conclusions

The main conclusions from this work can be summarised as follows:

- ISO-LWS observations have led to the first detections of FIR molecular lines from three HAEBE stars (IRAS12496-7650, RCrA and LkH $\alpha$ 234) out of a sample of 11 objects.
- High-J CO pure rotational lines (from  $J_{\text{up}} = 14$  to  $J_{\text{up}} = 19$ ) have been detected in all the sources; some OH lines are present in RCrA and LkH $\alpha$ 234 spectra, while no evidence of water vapour emission has been revealed.
- The data have been consistently fitted with an LVG model. For all the objects the emission appears to originate in warm, dense gas, which is located in very compact regions.

- Where the OH lines are detected, the corresponding estimated abundance is about two orders of magnitude greater than the common values of the interstellar medium.
- Among all the stars of the sample, those sources which exhibit molecular lines have the highest densities ( $n_{\text{H}_2} \gtrsim 10^5 \text{ cm}^{-3}$ ). This favours an association between molecular emission and density peaks and, as a consequence, possible embedded companions of HAEBE stars.
- The photodominated mechanism in high density or clumpy environments appears to be the likely source of the excitation, while shocks can be reasonably ruled out, at least in the sources where OH emission is observed. These findings are supported by the simultaneous absence of water vapour lines and the overabundance of OH, circumstances which can only be fully explained in photodominated environments.

## References

- Bechis K.P., Harvey P.M., Campbell M.F., Hoffmann W.F., 1978, ApJ 226, 439
- Bergin E.A., Melnick G.J., Neufeld D.A., 1997, ApJ 499, 777
- Bohlin R.C., Savage B.D., Drake J.F., 1978, ApJ 224, 132
- Burton M.G., Hollenbach D.J., Tielens A.G.G., 1990, ApJ 365, 620
- Cabrit S., Lagage P.O., McCaughrean M., Olofsson G., 1997, A&A 321, 523
- Cantó J., Rodríguez L.F., Calvet N., Levreault R.M., 1984, ApJ 282, 631
- Chackerian C., Tipping R.H., 1983, J. of Molecular Spectroscopy 99, 431
- Clegg P.E., Ade P.A.R., Armand C., et al., 1996, A&A 315, L38
- Draine B.T., Roberge W.G., Dalgarno A., 1983, ApJ 264, 485
- Dent W.R., Sandell G., Duncan W.D., Robson E.I., 1989, MNRAS 238, 1497
- Di Francesco J., Evans II N.J., Harvey P.M., Mundy L.G., Butner H.M., 1998, ApJ 509, 324
- Elitzur M., de Jong T., 1973, A&A 67, 323
- Elitzur M., Watson W.D., 1978, A&A 70, 443
- Edwards S., Snell R.L., 1983, ApJ 270, 605
- Fuente A., Martín-Pintado J., Chernicharo J., Bachiller R. 1990, A&A 237, 471
- Fuente A., Martín-Pintado J., Chernicharo J., Brouillet N., Duvert G., 1992, A&A 260, 341
- Fuente A., Martín-Pintado J., Bachiller R., Neri R., Palla F., 1998, A&A 334, 253
- Graham J.A., 1993, AJ 105, 561
- Habing H.J., 1968, Bull. Astr. Inst. Netherlands 19, 421
- Harju J., Haikala L.K., Mattila K., et al., 1993, A&A 278, 569
- Henning T., Launhardt R., Steinacker J., Thamm E., 1994, A&A 291, 546
- Henning T., Burkert A., Launhardt R., Leinert Ch., Stecklum B., 1998, A&A 336, 565
- Hollenbach D., Mc Kee C.F., 1989, ApJ 342, 306
- Hughes J.D., Hartigan P., Graham J.A., Emerson J.P., Marang F., 1991, AJ 101, 1013
- Irvine W.M., Goldsmith P.F., Hjalmarsen A.H., 1987, In: Hollenbach D.J., Thronson H.A. (eds.) *Interstellar Processes*
- Kaufman M.J., Neufeld D.A., 1996, ApJ 456, 250
- Kessler M., Steinz J.A., Anderegg M.E., et al., 1996, A&A 315, L27
- Knee L.B.G., 1992, A&A 259, 283
- Kylafis N.D., 1991, In: Lada C.J., Kylafis N.D. (eds.) *Proc. of The Physics of Star Formation and Early Stellar Evolution*, p. 269
- Lada C.J., Blitz L., Reid M.J., Moran J.M., 1981, ApJ 243, 769
- Levreault R.M., 1988, ApJS 67, 283
- Loren R.B., Sandqvist A., Wotten A., 1983, ApJ 270, 620
- Lorenzetti D., Tommasi E., Giannini T., et al., 1999, A&A, this issue (Paper I)
- McKee C.F., Storey J.W.V., Watson D.M., Green S., 1982, ApJ 259, 647
- Melnick G.J., Genzel R., Lugten J.B., 1987, ApJ 321, 530
- Mitchell, G.F., Matthews, H.E., 1994, ApJ 423, L55
- Mundt R., Ray T.P., 1994, ASP Conference Series 62, 237
- Nisini B., Benedettini M., Giannini T., et al., 1999, A&A 343, 255
- Nisini B., Lorenzetti D., Cohen M., et al., 1996, A&A 315, L321
- Offer A.R., van Dishoeck E.F., 1992, MNRAS 257, 377
- Prusti T., Natta A., Palla F., 1994, A&A 292, 593
- Ray T.P., Poetzel R., Solf J., Mundt R., 1990, ApJ 357, L45
- Reipurth B., Chini R., Krügel E., Kreysa E., Sievers A., 1993, A&A 273, 221
- Rodríguez L.F., Moran J.M., Ho P.T.P., Gottlieb E.W., 1980, ApJ L35, 845
- Rothman L.S., Gamache R.R., Goldman A., et al., 1987, Appl. Opt. 26, 4058
- Sandell G., Olofsson H., 1981, A&A 99, 80
- Saraceno P., Nisini B., Benedettini M., et al., 1998, In: Yun J.L., Liseau R. (eds.) *Proc. of Star Formation with the Infrared Space Observatory*. ASP Conf. Series vol.132, p. 233
- Scappini F., Palumbo G.G.C., Bruni G., Bergmann P., 1994, ApJ 427, 259
- Skinner S.L., Brown A., Stewart R.T., 1993, ApJS 87, 217
- Swinyard B.M., Clegg P.E., Ade P.A.R., et al., 1996, A&A 315, L43
- Taylor K.N.R., Storey J.W.V., 1984, MNRAS 209, 5P
- van Dishoeck E., Dalgarno A., 1984, Icarus 59, 305
- Weintraub D.A., Kastner J.H., Mahesh A., 1994, ApJ 420, L87
- Wilking B.A., Harvey P.M., Joy M., Hyland A.R., Jones T.J., 1985, ApJ 293, 165
- Wilking B.A., McCaughrean M.J., Burton M.G., et al., 1997, AJ 114, 2029